ELSEVIER

Fusion Engineering and Design 39–40 (1998) 287–294

Fusion Engineering and Design

Response of plasma-facing materials to high transient heat loads in a tokamak

H. Bolt [a,*], T. Scholz [a], J. Boedo [b], K.H. Finken [a], A. Hassanein [c], J. Linke [a]

[a] *Forschungszentrum Jülich GmbH, Association EURATOM-KFA, D-52425 Jülich, Germany*
[b] *University of California, Fusion Energy Program, San Diego, CA 92093, USA*
[c] *Argonne National Laboratory, Fusion Power Program, Argonne, IL 60439, USA*

Abstract

High transient heat loads to plasma-facing components, as they occur during plasma disruptions, edge localized modes (ELMs), or vertical displacement events, can cause damage such as thermal erosion, cracking, or melting. The incidence of high heat flux from a plasma onto a material surface triggers a sequence of dynamic plasma–material interaction processes of a non-linear character, commonly termed 'vapour shielding'. As a consequence, the further incident heat flux and the resulting ablation are strongly reduced. To study these effects, fast probe experiments were carried out in the TEXTOR tokamak. The materials exposed to the plasma were carbon fibre composites with and without silicon addition. The duration of the plasma exposure was 80 ms at a depth of up to 9 cm into the boundary plasma. Together with a strong decrease of the electron temperature in the boundary plasma, strongly localized emission of radiation was observed in front of the probe tip. The incident heat flux to the probe was strongly reduced, which was also found as result of numerical modelling of the local shielding processes.

1. Introduction

During the operation of tokamak fusion devices, instabilities of the plasma can occur which cause the deposition of transient high heat fluxes to the plasma-facing components. Events such as edge localized modes (ELMs), vertical displacement events (VDEs) and disruptions lead to increased fluxes of plasma particles on local areas, especially on divertor and limiter surfaces. In a next-generation tokamak such as the International Thermonuclear Experimental Reactor (ITER), the theoretical thermal energy deposition in such cases can be of the order of 10–150 MJ m^{-2} on a time scale of 1–300 ms, depending on the kind of plasma instability [1]. The material damage and the thermal ablation resulting from such heat loads would limit the lifetime of the plasma-facing components and require impracticably short maintenance intervals. In recent years, however, investigations employing laboratory experiments [2–4] and numerical analyses [5–9] were carried out, which indicate that shielding processes may take place in front of the highly heat loaded material surface so that only a fraction of the incident energy density is actually deposited in the material and that the major part

* Corresponding author. Tel.: +49 2461 614657; fax: +49 2461 613699.

0920-3796/98/$19.00
PII S0920-3796(98)00130-6

of the incident energy is dissipated to larger surface areas by radiation processes. As a consequence, the material damage and ablation can be reduced strongly. The effects which are responsible for the shielding of the loaded material surface are mostly caused by atoms and clusters of eroded matter which form a strongly radiating local cloud in front of the heated surface. In addition, transport of the eroded particles within the torus leads to increased energy loss by radiation of the plasma boundary and thus to a reduction of the boundary plasma temperature [9,10].

Experiments in the TEXTOR tokamak have been carried out to investigate the plasma–material interaction processes which take place, if a material surface is transiently exposed to a high incident heat load from the plasma. The aim of the investigation was to measure the local shielding which occurs directly in front of the material surface as well as the cooling effect which takes place throughout the plasma boundary. The experiments were carried out by mounting specimens of carbon fibre composite (CFC) with and without Si-addition to the tip of a fast reciprocating probe (UCSD-probe). Results of initial experiments on a different carbon material which describe the evolution of the discharge parameters in the plasma boundary were reported by Scholz et al. [9]. For the present paper, local measurements were carried out in the vicinity of the probe tip by optical emission spectroscopy and by fast CCD camera measurements. The local measurements were compared with numerical calculations of the ablation, vapour cloud evolution and local radiation processes. For the calculations, an upgraded version of the A*THERMAL-S code was applied [11].

2. Experimental

The exposure of material specimens to high heat fluxes from a tokamak plasma was performed by using a pneumatically driven fast probe of the UCSD team which is mounted on the TEXTOR tokamak. The duration of the in and out movement was about 20 ms each. The dwell time at the end position was 80 ms with the material specimen being introduced into the TEXTOR tokamak plasma up to a depth of 9 cm in front of the main limiter radius ($r_{\mathrm{min,probe}} = 37$ cm, $r_{\mathrm{limiter}} = 46$ cm). The specimens had a quadratic cross-section of 16×16 mm with a length of 120 mm. The probe tip was at floating potential and electrically isolated from other components. The probe was inserted into the plasma such that two specimen faces were placed perpendicular to the magnetic field lines and thus received the highest incident heat fluxes compared to the specimen surfaces aligned parallel with the magnetic field.

For the experiments described here, two CFC materials were used, SEP N11, a two-dimensional felt CFC with needling reinforcement and high thermal conductivity ($\rho = 1.76$ g cm^{-3}, $\lambda_{\mathrm{RT}} = 180$ W m^{-1}K^{-1} across planes, $\lambda_{\mathrm{RT}} = 220$ W m^{-1}K^{-1} in plane) and SEP NS11, a similar CFC with 10% Si added during the impregnation process ($\rho = 2.2$ g cm^{-3}, $\lambda_{\mathrm{RT}} = 180$ W m^{-1} K^{-1} across planes, $\lambda_{\mathrm{RT}} = 200$ W m^{-1} K^{-1} in plane).

The effects of the probe insertion on the evolution of the plasma parameters in the plasma boundary were investigated by HCN-interferometry and by He-beam diagnostics for electron density and temperature measurements. Measurements of the local emission of the radiation directly at the material probe were carried out by local optical emission spectroscopy (OES). This measurement allowed detection of thermal continuum radiation as well as line radiation emitted from neutral C-atoms ($\lambda = 908.85$ nm, 909.48 nm, $3s^3P^0$–$3p^3P$) which were eroded from the probe surface. The local observation area at the probe had a diameter of 1 cm and was adjusted to a radial position of $r = 42$ cm.

For the fast imaging of the radiating cloud which forms in front of the specimen surface during plasma exposure, a high-speed CCD camera was used with a frame rate of 330 s^{-1} and an infrared filter ($\lambda > 950$ nm) to observe thermal continuum radiation. With this camera, a field of 3×3 cm in front of the specimen shaft was observed. The observation field covered the radial positions of $r = 44$–41 cm. Before the experiments the CCD camera was calibrated with a white-light lamp.

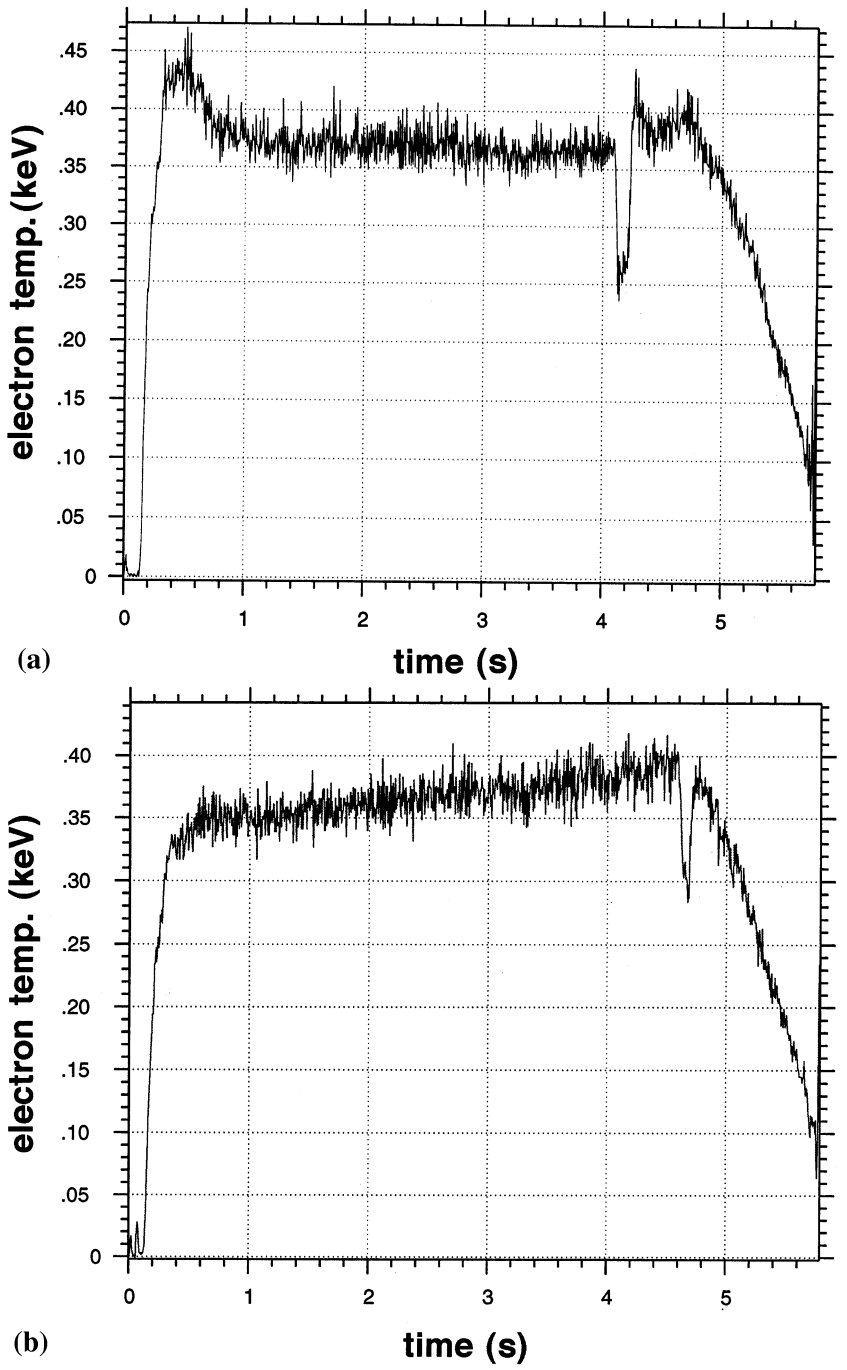

Fig. 1. ECE measurements of electron temperature at $r = 37$ cm: (a) discharge # 64246, insertion of N11 to $r = 37$ cm at 4.1 s; (b) discharge # 64386, insertion of NS11 to $r = 40$ cm at 4.6 s.

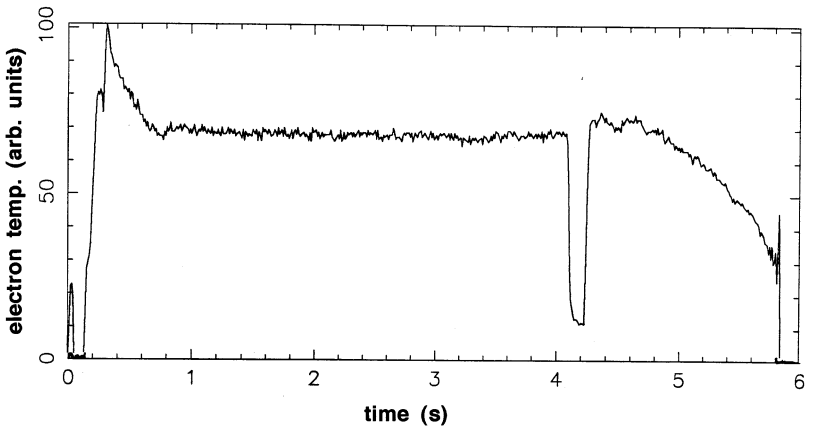

Fig. 2. He-beam measurement of the electron temperature at $r = 43$ cm; discharge # 64246, insertion of N11 to $r = 37$ cm at 4.1 s.

3. Experimental results

3.1. Plasma boundary processes

The tests of the N11 material and of the Si-containing NS11 material were carried out in ohmic plasma discharges of similar characteristics, i.e. plasma density and temperature profiles before probe insertion. The N11 specimen was introduced to a depth of 9 cm in front of the main limiters without causing plasma disruptions (10 shots). With the Si-containing NS11, most exposures (30 shots) were performed at an insertion depth of 6 cm to avoid the occurrence of disruptions. The corresponding plasma parameters electron temperature, T_e, electron density, n_e, and heat fluxes, q, of the undisturbed plasma in the tip region of the probe were: for N11 (9 cm penetration), $T_e = 300–350$ eV, $n_e = 5 \times 10^{12}$ cm^{-3}, $q =$ 23 kW cm^{-2}; and for NS11 (6 cm penetration), $T_e = 150$ eV, $n_e = 5 \times 10^{12}$ cm^{-3}, $q = 8.5$ kW cm^{-2}. For the calculation of q, an energy transmission factor of 8 was assumed [10].

During the insertion of the probes, material is thermally eroded under the incident heat flux, which causes an increase of the impurity radiation in the edge boundary [9]. This energy loss leads to a reduction of the plasma edge temperature during the probe insertion (Fig. 1). Both for the N11 and NS11 materials, the electron temperature measured by ECE at a minor radius of $r = 37$ cm is reduced by about 20–30%. For N11 this reduction is more significant, since the probe tip had been inserted up to $r = 37$ cm and NS11 was only introduced up to $r = 40$ cm.

Further into the shadow of the probe ($r = 43$ cm), the decrease of the electron temperature is much stronger as the results of He-beam measurements of the electron temperature show (Fig. 2). Before probe insertion, the electron temperature at this position was about $T_e = 80$ eV with a very strong decrease upon insertion of the probe. Due to the simultaneous increase of the electron density in the plasma edge, the T_e value measured during probe insertion cannot be given in absolute values, but the measurement shows that the plasma edge temperature in the shadow of the probe and, thus, also the incident heat flux from the plasma decrease drastically.

3.2. Local processes near the probe surface

In the direct vicinity of the probe, the OES measurement in the range of $\lambda = 907–910$ nm shows a distinct sequence in which continuum and line radiation are detected (Fig. 3). This sequence can be explained by the motion of the hot probe tip through the observation area during the inward and the outward stroke of the probe. With the tip staying in the end position, only the vicin-

ity of the probe shaft at $r = 42$ cm can be observed. Since the probe shaft is obviously not hit by high heat flux due to the strongly reduced electron temperature in this region, the shaft remains cold and does not emit thermal radiation nor C-impurities which could emit line radiation. The line radiation from eroded neutral C-atoms, together with intense continuum radiation, appears only when the hot tip is moved through the observation area. When being withdrawn from the plasma at $t = 4.26$ s, the tip is heated to a higher temperature and emits more radiation than during the movement into the plasma at $t = 4.12$ s.

The calibrated CCD camera measurements gave further insight into the local shielding processes near the probe tip. Fig. 4 shows a sequence of five images during the inward stroke of the probe tip. In the images, the material surface of the hot probe tip passes on the left edge of the frames. In front of the hot probe tip, a local and strongly radiating zone of 10–20 mm extension develops which travels, together with the hot tip, downward through the observation field. Between the in and out sequences, no radiation was detected for 100 ms, which is the dwell time of the probe in the end position plus the time of the probe tip needed to travel from the observation field to the end position and vice versa. The radiation pattern measured during the outward stroke of the probe tip is similar, but more intense.

The temperature in the centre of the observed cloud as derived from the radiation intensity measured with the CCD camera was 3600 K. Thus the cloud temperature is higher than the surface temperature of the exposed material, which can be calculated from the measured material erosion to be approximately 3000–3200 K [10].

4. Numerical results

The numerical simulation of shielding effects in front of the heated target was performed by calculating the ablation as a function of the incident heat flux and the resulting carbon vapour density distribution in front of the substrate. Based on this, the stopping power of the vapour and the radiation emission was calculated transiently under moving boundary conditions in a one-dimensional finite element mesh up to 10 cm in front of the heated carbon surface. Because of the importance of radiation transport in the

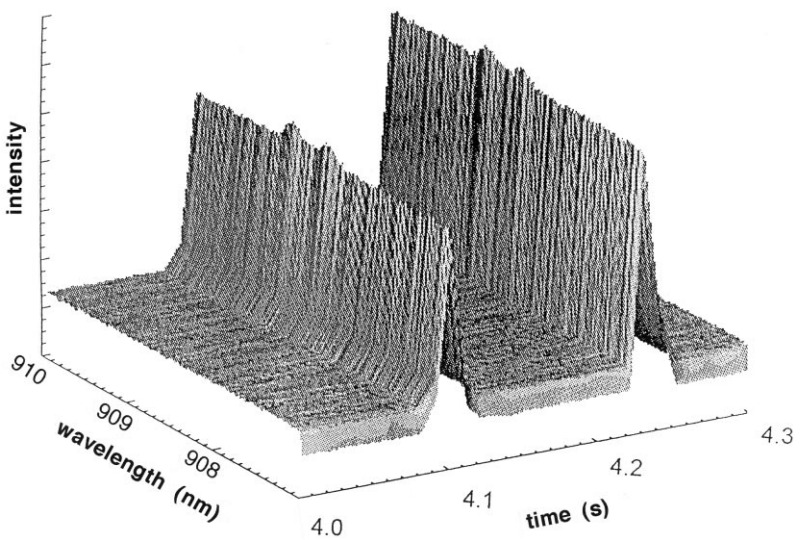

Fig. 3. Radiation in the range of $\lambda = 907$–910 nm emitted at $r = 42$ cm in the direct vicinity of the probe surface, discharge # 64246.

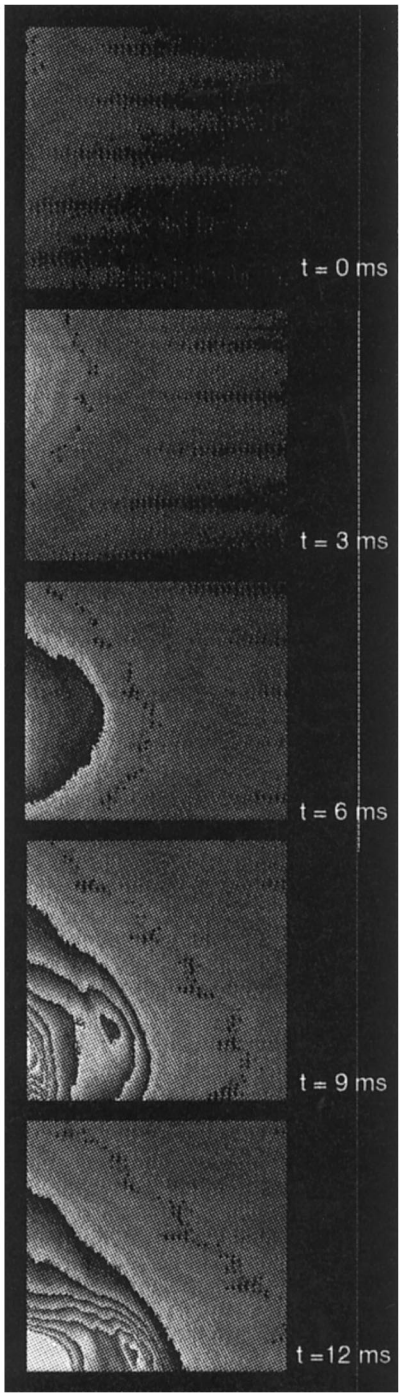

Fig. 4. Sequence of CCD camera images of probe insertion into discharge #64386, material NS11 (inward stroke). The moving probe surface passes the image frame on the left side. Strong continuum radiation is emitted in front of the probe surface as the probe is increasingly heated by the plasma, and ablation occurs (frames at 9, 12 ms).

dense vapour cloud, the actual radiation field in the cloud was determined for each time step from the balance of radiation emission and absorption. A detailed description of the complex features of the code can be found in Hassanein and Konkashbaev [6].

From the time-resolved calculations, it was found that during the exposure of the CFC material, a quasi-equilibrium of energy shielding and energy transmission by radiation from the incident plasma to the probe surface was reached. The radiation spectra towards the probe surface and in the direction of the vacuum vessel during this steady-state condition are shown in Fig. 5(a) and (b) for an incident heat flux from the plasma of 22 kW cm^{-2}. Because of the radiation transport taking place within the dense vapour cloud, the intensity of the radiation into the vacuum is about 10 times higher than the radiation towards the probe surface. This is caused by the radiation of higher energy photons (>10 eV) at the outer cloud edge, which are produced by the interaction of the hotter plasma particles with the cloud particles.

In Fig. 5(a) the sensitivity range of the CCD camera is noted on the x-axis. By comparing the radiation intensity in this range with the measured intensity, good agreement is found, since the calculation also predicts radiation corresponding to a black body temperature of 3600 K.

5. Summary

Pure and Si-containing CFC materials were exposed to incident heat fluxes of up to 23 kW cm^{-2} in the TEXTOR tokamak for durations of approximately 80 ms. The thermal ablation of material caused strong plasma radiation and thus decreased the electron temperature in the boundary plasma, which resulted in a reduction of the incident heat flux.

The local measurements using OES and CCD camera imaging allowed direct observation of the local vapour shield effect in front of plasma-exposed materials in a tokamak. The efficiency of the vapour shielding in reducing the incident heat

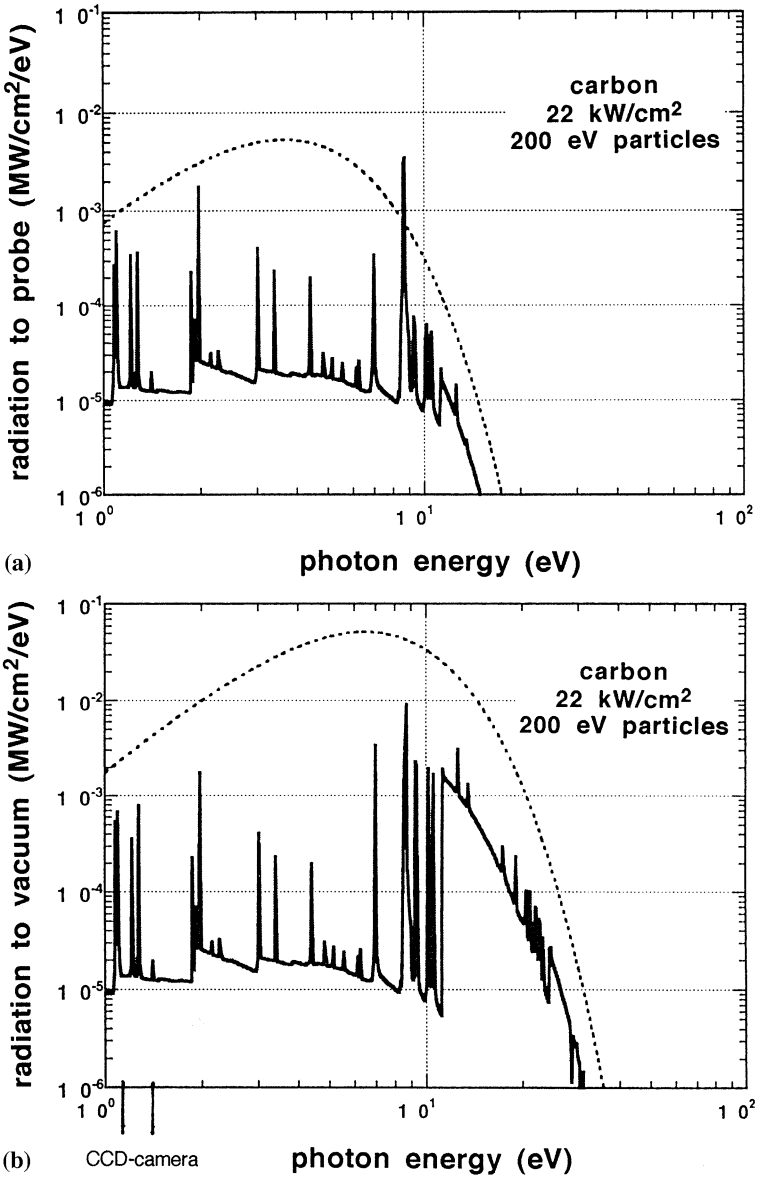

Fig. 5. Calculated radiation spectra of the vapour cloud in front of the probe, incident heat flux from plasma $q = 22$ kW cm^{-2}. Dotted line gives envelope for black body radiation. (a) Radiation spectrum from vapour cloud towards vacuum vessel; (b) radiation spectrum from vapour cloud towards the specimen surface.

flux was also verified by numerical calculations of the local plasma–material interaction processes which showed quantitative agreement in terms of the radiation intensity of the vapour cloud as it has been measured by the CCD camera.

Acknowledgements

The authors greatly appreciate the support and help of the plasma diagnostic group at TEXTOR.

References

[1] R.R. Parker, W.B. Gauster, Fusion Eng. Des. 30 (1995) 119.
[2] J.M. Gahl, J.M. McDonald, A. Zakharov, S. Tserevitinov, V. Barabash, M. Guseva, J. Nucl. Mater. 191/194 (1992) 454–459.
[3] H. Bolt, V. Barabash, A. Gervash, J. Linke, H. Nickel, I. Ovchinnikov, M. Rödig, Fusion Eng. Des. 30 (1995) 225–232.
[4] J. Linke, V.R. Barabash, H. Bolt, A. Gervash, I. Mazul, I. Ovchinnikov, M. Rödig, J. Nucl. Mater. 212/215 (1994) 1195–1200.
[5] J. Gilligan, D. Hahn, R. Mohanti, J. Nucl. Mater. 162/164 (1989) 957–963.
[6] A. Hassanein, I. Konkashbaev, in: Atomic and Plasma–Material Interaction Data for Fusion, vol. 5, International Atomic Energy Agency, Vienna, 1994, p. 193.
[7] H. Bolt, H. Harano, H. Madarame, K. Okamoto, H. Takabe, J. Nucl. Mater. 196/198 (1992) 948–952.
[8] H. Würz, N.I. Arkhipov, V.P. Bakhin, et al., J. Nucl. Mater. 212/215 (1994) 1349–1352.
[9] T. Scholz, J. Boedo, H. Bolt, R. Duwe, K.H. Finken, D. Gray, A. Hassanein, J. Nucl. Mater. 241–243 (1997) 848.
[10] T. Scholz, J. Boedo, H. Bolt, K.H. Finken, H. Nickel, Report Forschungszentrum Jülich, Jül-3314, December 1996.
[11] A. Hassanein, I. Konkashbaev, J. Nucl. Mater. 233/237 (1996) 713.